Assessment of Structural Requirements for Crossing Panel Design using Dynamic Load Case Scenarios

H. Vilhelmson, B. A. Pålsson and J. C. O. Nielsen

Department of Mechanics and Maritime Sciences / CHARMEC, Chalmers University of Technology, Gothenburg, Sweden

Abstract

Structural requirements for railway crossing panel design are proposed. These include dynamic load scenarios established from field measurements and structural load limits for the crossing rail, sleepers and maximum allowed vertical contact stress on the ballast surface. Using a simulation environment with two track models of varying detail, the structural load limits are challenged using the dynamic load scenarios. The two-layer track models include stock rails and sleepers represented by beam elements and a crossing rail represented by either 3D solid elements or beam elements. Linear bushings are used for the rail fastenings and bi-linear bushings for the ballast to allow for potentially voided sleepers. The applied load scenarios are established by combining measured data from scanned hollow worn wheel profiles, scanned crossing rail geometries, and sleeper-ballast voids extracted by calibrating a track model to measured sleeper accelerations. The study shows that the highest dynamic wheel-rail contact loading is achieved for a geometry where a nominal crossing rail geometry (virgin rail profile) is combined with a hollow worn wheel profile. The study provides an understanding of what field conditions the crossing panel could be subjected to before the loading exceeds the load limits of the components. It is foreseen that the data presented in this paper can be used for optimisation of crossing panel design while considering dynamic loading.

1 Introduction

A fixed crossing allows for trains to cross intersecting tracks. In the wheel transfer from wing rail to crossing nose (or vice-versa), the conicity of the wheel in combination with the variation in rail geometry along the crossing results in a wheel–rail excitation that is characterised by a dip in the vertical wheel trajectory. This leads to wheel–rail impact loading that may cause severe deterioration of the crossing panel, for example in terms of wear, plastic deformation and rolling contact fatigue (RCF) of the crossing rail, sleeper cracking and differential settlement of ballast.

To reduce this deterioration and improve the long-term performance, the optimisation of switches & crossings (S&Cs) has been a topic of interest in recent years [1–5]. Generally, one component at a time has been considered and the main focus has been on reducing the wheel–rail contact forces. In [2], the running surface geometry of the crossing rail was optimised to minimise the maximum Hertzian wheel–rail contact pressure for a representative set of wheel profiles. The most common approach focuses on optimising the rail fastening stiffness to decrease deterioration related to some of the most common failure modes. Examples considered in the literature include wear, RCF, differential settlement and fatigue of the track components studied in [3], wheel–rail contact forces, rail seat loads in [4], and loads on the ballast in [5]. All studies mentioned assume that as the wheel–rail contact force is reduced, then so is the structural loading and the life-span of the S&C is increased. Thus, the structural requirements of the S&Cs do not need to be considered. This includes the dynamic loading that the design should be dimensioned against and structural load limit for each component. However, in a structural optimisation that allows for significant changes in the design of the components, this assumption is no longer valid. This increases the complexity of the optimisation problem, but it also introduces the possibility to further improve the performance of the crossing panel by optimising the size, topology or material of the components. The added complexity comes mainly from that structural requirements must be established and adhered to. The dynamic loading scenario is especially difficult to quantify since it may vary substantially over the life of the crossing panel as support conditions, wheel–rail contact geometry and traffic conditions change. In an optimisation problem it is not feasible to consider the dynamic vehicle–track interaction for entire life-span of the crossing panel. Instead, representative dynamic load scenarios can be formed.

One approach used in industry to establish a representative worst case dynamic load scenario for a specific traffic situation is to disregard irregularities in sleeper support conditions but use a hollow worn wheel profile, which is a relatively common and well established deterioration pattern. A nominal crossing rail geometry is generally considered as the deterioration pattern seen in crossing rails may vary depending on crossing angle, vehicle speeds, axle loads, etc. From the combined wheel–rail ge-

ometry, a kinematic dip angle is calculated and used in the Jenkins formula for the so-called P2-force [6]. In this paper, the ambition is to account for different wheel profiles, deterioration patterns of the crossing panel and sleeper support conditions when the various dynamic loading scenarios are established.

This paper aims to provide a framework for structural optimisation of the crossing panel by establishing structural requirements for the S&Cs based on studied field conditions and design requirements. In addition, the aim is to assess the structural load limits by applying the established dynamic load scenarios on simulation models of a reference crossing panel design developed and validated in [7, 8].

2   Simulation model

The crossing panel model is based on the 60E1-500-1:12 demonstrator installed in the Austrian network as a part of the In2Track projects in the EU-funded Shift2Rail research programme [9]. A structural finite element model of the crossing panel is implemented in the commercial MBS software Simpack using substructures generated by Craig-Bampton model reduction [10] from individual finite element models of the crossing rail, stock rails and sleepers, respectively. It is a two-layer track model with stock rails and sleepers represented by beam elements. In two different models, the crossing rail is modelled using either beam elements or 3D solid elements, see Figure 1 for an illustration of the 3D track and vehicle model. The 3D mesh of the crossing rail, see Figure 2, uses quadratic elements and a mesh refinement near the most loaded section of the ribs (near the crossing transition area) on the bottom surface of the rail. The model incorporates scanned crossing rail geometries from in-situ crossings. The track model uses linear bushings for the rail fastenings and bi-linear bushings for the ballast to allow for potentially voided sleepers. The rail fastenings have varying stiffness depending on placement. The fastenings below the crossing rail have a stiffness of 25 MN/m, while the remaining fastenings have a stiffness of 50 MN/m.

Large variations in in-situ track bed modulus (combined stiffness for ballast and subgrade) can be expected. As reported in [11], values measured with track recording cars (TRCs) range from about 90 MN/m^3 to 200 MN/m^3. More recent experimentally determined values using either TRCs or track instrumentation can be found in [12, 13]. Here, the track bed modulus ranged from about 30 MN/m^3 to 140 MN/m^3. As found in the literature on the subject, values used in simulation work generally vary within similar ranges. For example, in the S&Cs benchmark a value of 60 MN/m^3 was used [14]. In [7, 8], based on extensive field measurements in the Shift2Rail crossing demonstrator in Austria, the track bed modulus was calibrated to 120 MN/m^3. This is the bed modulus that will be used in this paper.

The vehicle model is a bogie based on the Manchester benchmark passenger vehicle model [15], with modified suspension, mass and wheelbase to fit each loading scenario. For each evaluated track configuration, the initial conditions of the vehicle and track models are determined by evaluating the static equilibrium for the vehi-

3

cle–track system before the start of each time-domain simulation. In this paper, only the through route is simulated.

A plain line reference track section is also created to allow for comparisons of structural loading between S&C and plain line. In this reference case, the rail pad stiffness is set to 100 MN/m. All other simulation parameters are identical to the crossing panel model.
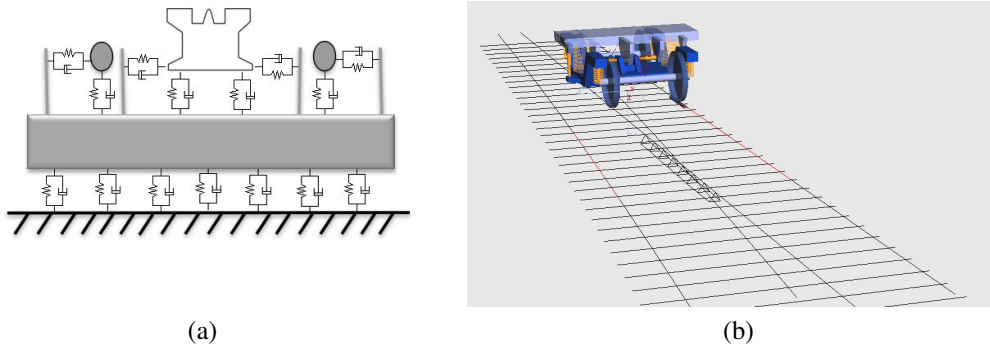

(a)   (b)

Figure 1: a) Illustration of a cross-section of the 3D track model at a sleeper. b) Full crossing panel model and vehicle model.
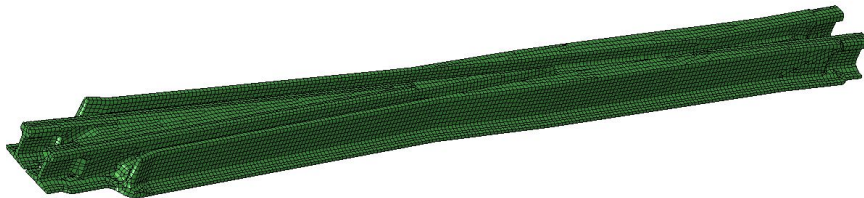

Figure 2: Overview of the complete 3D crossing rail model.

3 Structural requirements

To enable structural optimisation of the crossing panel, structural requirements must be determined. These include, dynamic loading scenario and the load limits of the components. The dynamic loading scenario is specified by a traffic load case and track deterioration case. The traffic load case determines the axle loads and train speeds that the crossing panel should be dimensioned against, while the load limits of the components specify the structural loading each component can be subjected to

4

before failure. Based on studied field measurements, the deterioration cases quantify various states that heavily affect the dynamic vehicle–track.

3.1 Traffic load cases

For the S&Cs requirements used in the Swedish railway network, standardised traffic load scenarios (combinations of train speeds and axle loads) have been specified as, [16],

(A) 60 km/h and 30 tonne axle load
(B) 120 km/h and 25 tonne axle load
(C) 250 km/h and 19.5 tonne axle load

For a 1:12 crossing, there is however another standard [17] that limits the train speed in the through route to 200 km/h. Thus, this speed has been used as the dimensioning speed in scenario C. The three scenarios have been studied in simulations assuming nominal conditions for the wheel–rail contact geometry and sleeper support. It was then found that the worst case scenario for the structural loading of all components is A, except for sleeper bending stress where scenario B showed slightly higher values. Thus, scenario A has been used in all subsequent simulations in this paper.

3.2 Load limits of crossing panel components

3.2.1 Sleeper fatigue limit

As specified in [18], a sleeper in the crossing panel should hold up for a bending moment of $M = \pm 25$ kNm without crack initiation [19]. Since bending moment is not suitable to use as a constraint in a structural optimisation as it neglects the effect from a potential change in shape, it has been recalculated to tensional stress on the surface of the sleeper. Using Euler-Bernoulli beam theory and considering the geometry of an existing sleeper design where this requirement is applicable, the calculated stress limit is

$$g_{\sigma,\text{sleeper}} = \frac{Mh_{sl}}{I} = 10.56 \ \text{MPa} \tag{1}$$

where $I = 2.57 \cdot 10^{-4} \ \text{m}^4$ is the second moment of area of the weakest sleeper cross-section and $h_{sl} = 0.109$ m is the distance from the centre of gravity to the bottom of the sleeper for the same cross-section.

3.2.2 Sleeper–ballast contact pressure limit

The most common damage mode related to sleeper–ballast contact pressure is ballast settlement. Several models to predict differential settlement of ballast have been presented in the literature, see for example the review papers [20, 21]. In some models, the increment in settlement per load cycle (passing wheelset) is taken as zero unless a threshold value in terms of maximum sleeper–ballast contact pressure is exceeded. An

experimentally derived threshold value for ballast settlement can be found for example in [22], where the threshold value was determined to be 139 kPa. However, the threshold value is site specific and depends on for example the quality and material of the ballast and the properties of the embankment and foundation. Other models assume that incremental settlement occurs independent of the magnitude of sleeper–ballast contact pressure. Common for many ballast settlement models is that the settlement does not vary linearly, but that the settlement often increases exponentially with the increase of sleeper–ballast contact pressure. In this paper, it is assumed that a low rate of ballast/subgrade settlement is unavoidable (and acceptable).

In [23], the load bearing capacity of ballast is determined by specifying a maximum admissible pressure on the ballast bed. It is given as $\sigma_{\text{ballast}} = 500$ kPa. This is a value commonly considered by the Swedish Transport Administration, but a more conservative limit of the load bearing capacity 300 kPa is used for macadam class 1 $(31.5 - 63$ mm$)$ ballast, which is the maximum admissible pressure on the ballast bed given in [24]. However, due to the difficulty in measuring the ballast pressure and correlating it to damage and settlement rates, no official limit has been specified.

As mentioned above, the Swedish Transport Administration sets no limit for maximum sleeper–ballast contact pressure. However, the alarm limit for wheel–rail contact force used in plain track is 350 kN [25]. From this, it is suggested that an implicit maximum allowable ballast pressure for plain track can be determined as a reference. By comparing simulations with a plain track model and the crossing panel model with nominal conditions of wheel–rail contact geometry and sleeper support, it was found that both track forms lead to similar sleeper–ballast contact pressures, see Table 1. As the ballast for both cases are comparable, it is assumed that if a maximum limit can be established for plain track, it should also be representative for the crossing panel.

Thus, by using the plain track model with nominal sleeper support conditions, the simulation of traffic load scenario A has been extended to include a wheelflat (with calibrated length ≈ 100 mm and depth = 2.3 mm) leading to a 350 kN impact force at the same longitudinal distance from the adjacent sleeper as where the crossing impact occurs in the crossing panel model. This resulted in a maximum sleeper–ballast contact pressure of 347 kPa, see Table 1, which is similar to the permissible stress specified in [24]. However, as the wheel–rail contact force limit is specified for plain track, it should be considered that this limit is not intended for repeated loadings at the same position along the track. With this in mind a more conservative version of this limit should be considered for crossing panels. In this paper, the load limit $g_{\sigma,\text{ballast}}$ is set to 300 kPa. However, in an optimisation, the settlement should also be accounted for by choosing a suitable settlement model as a penalty function.

3.2.3 Crossing rail fatigue limit

In industrial applications of crossing rail design, a Deutsche Bahn document [26] is sometimes used as an inofficial standard. It sets the fatigue limit for rail foot stresses to 200 MPa. However, this value is not tuned for a manganese steel crossing rail.

Model	σ_{ballast} [kPa]
Nominal crossing	143
Nominal plain track	138
Wheelflat plain track	347
Limit value [24]	300

Table 1: Sleeper–ballast contact pressure for different load case scenarios and the limit value.

According to [26], the tensile strength for UIC 60 steel is 900 MPa. The reduction factor given as the ratio between fatigue limit and tensile strength is then calculated as 0.22. Based on the same reduction factor and a tensile strength for manganese steel of 780 MPa, the bending fatigue limit for manganese crossings would be calculated as $g_{\sigma,\text{crossing}} \approx 173$ MPa.

3.3 Deterioration cases

In order to establish a representative worst case scenario for the sleeper support conditions, the existing literature on the subject has been studied. Field measurements have indicated the presence of ballast voids or hanging sleepers [7, 27–30], while other studies have quantified the magnitude of voids by calibrating a simulation model to field measurements [7, 31]. Unfortunately, direct measurements of ballast voids in crossings are difficult to find in the literature. Thus, most of the pre-existing work attempting to quantify ballast voids in turnouts come from a combination of measurements and simulation work.

In [31], six crossing panels were studied in-situ. Sleeper acceleration was measured and reconstructed to displacement. A simulation model was then calibrated to determine the sleeper support conditions for each crossing panel. The calibration indicated between one and three hanging sleepers with voids in the interval 0.55 – 2 mm for three of the crossing panels. In particular, one crossing panel in a very poor condition was calibrated to have four hanging sleepers with a 5 mm void. Based on this information, worst case scenarios have been created. In Figures 3a and 3b, four different scenarios for the sleeper support conditions are shown. Case 1 represents a situation where four consecutive sleepers are voided with a uniform sleeper–ballast gap of 5 mm. This case is used as a worst case scenario for the bending stress in the crossing rail. Case 2 represents a situation where four consecutive sleepers are supported by a ballast shoulder in the through route. This case acts as a worst case scenario for the sleeper–ballast contact pressure. In Case 3, four consecutive sleepers are only supported in the diverging route, resulting in a worst case scenario for the sleeper bending stress. Based on the sleeper support conditions evaluated for the other crossing panels studied in [31], Case 4 was created with two hanging sleepers with a uniform sleeper–ballast gap of 2 mm. This case is intended to be a scenario which may be expected to occur more frequently, while the other cases are more extreme.

For each sleeper support condition and assuming traffic load scenario A in Section 2, the calculated maximum stress and sleeper–ballast contact pressure for the sleeper adjacent to the crossing transition, and the maximum crossing rail stress, have been calculated using the beam version of the crossing panel model. The results are compared with the corresponding outputs in case of nominal sleeper support conditions (no voids) in Table 2.
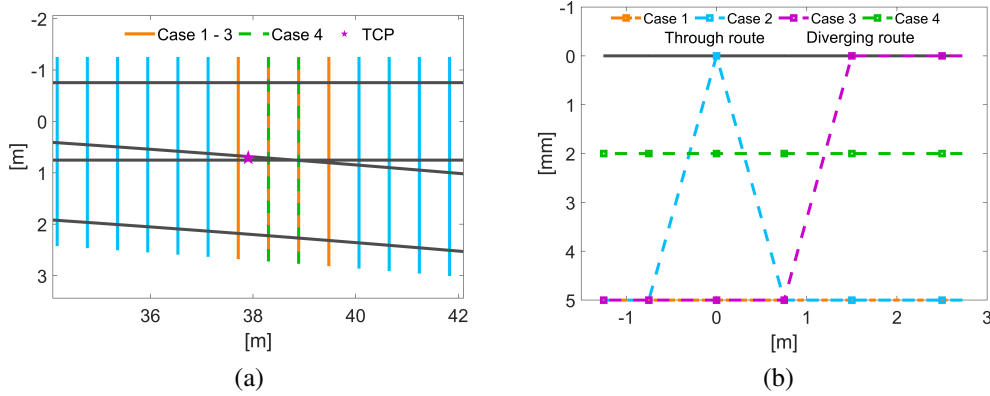

Figure 3: a) Discretisation of sleeper support conditions in the crossing panel. b) Four scenarios with different sleeper support conditions.

	k_{sleeper}	k_{ballast}	k_{crossing}	Sleeper support conditions
Nominal	1	1	1	Uniform ballast support
Case 1	1.27	0.96	1.72	Four sleepers, 5 mm void
Case 2	1.27	2.30	1.38	Four sleepers, ballast shoulder
Case 3	1.52	1.22	1.46	Four sleepers, partial support
Case 4	1.20	0.67	1.23	Two sleepers, 2 mm void
Normalised Limit value	2.08	2.09	2.93	

Table 2: Influence of sleeper support conditions on rail and sleeper stresses and sleeper–ballast contact pressure. The calculated values have been normalised with respect to corresponding values for the nominal case with uniform sleeper support. Orange text indicates the critical support condition for each response that will be used in the subsequent analysis.

As discussed above, another situation significantly affecting the dynamic loading in the crossing panel is the combination of wheel and rail contact geometry. In operation, the transition area of the crossing rail may be subjected to severe deterioration in the forms of wear and plastic deformation. The magnitude of this deterioration may vary significantly between different turnouts depending on traffic conditions, such as axle loads and train speeds, as well as on crossing type and placement (curve radius, etc.). To include this aspect in the simulations, measured transition geometries of in-situ crossings are used. Running surface geometries of crossing rails that have

8

been subjected to 0, 65 and 120 MGT of traffic load have been scanned. The 65 MGT crossing was however situated in a curve leading to higher deterioration than on tangent track [32]. These three crossing rail geometries have been combined with four scanned wheel profiles, one with a nominal wheel profile while three profiles were hollow worn with different amounts of wear. The rail profiles generated from the scanning of the nominal crossing rail (0 MGT) and all considered wheel profiles are shown in Figures 4a and 4b, respectively. The calculated normalised structural loading for each component, k_{sleeper}, k_{ballast}, k_{crossing} using the beam version of the model is listed in Table 3. The combination of wheel and rail contact geometry leading to the most severe loading is highlighted in the table.
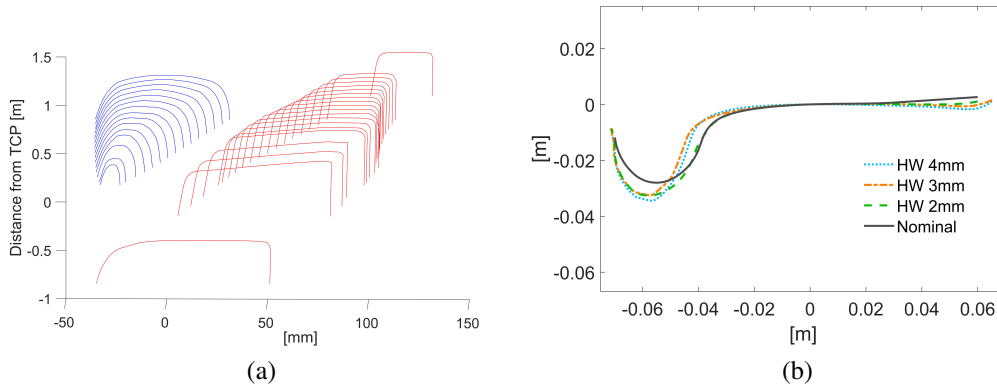

Figure 4: a) Scanned nominal crossing rail geometry. b) Scanned wheel profiles.

For the hollow worn wheel profiles with 3 and 4 mm of wear, it can be observed in Table 3 that the normalised structural loading is higher for the nominal rail geometry (0 MGT) than for the worn rail geometries (65 and 120 MGT). The dip angle β, which as discussed above is commonly used to calculate the dynamic load analytically, can be evaluated from the calculated vertical wheel trajectory in each simulation. The dip angle has been calculated by considering two linear regression lines constructed with data from 10 cm on either side of the minimum point of the dip. In Table 3, it is observed that the dip angle is generally increasing with increasing wear of the hollow worn wheel profiles.

4   Assessment of structural load limits

Each of the severe sleeper support conditions (Cases 1 – 4 in Table 2) are paired with the most severe combination of wheel and rail contact geometry highlighted in Table 3 (nominal crossing rail geometry and a hollow worn wheel profile with 4 mm of wear) to form three worst case dynamic load scenarios (one for each structural requirement in Section 3) and a fourth case aiming to represent more realistic operational conditions. The simulation results for these four constructed cases (Cases I – IV) are

Wheel geometry	MGT	k_{sleeper}	k_{ballast}	k_{crossing}	β [mrad]
Nominal	0	1	1	1	7.93
2 mm hollow	0	1.24	1.08	1.25	15.36
3 mm hollow	0	1.50	1.23	1.40	23.10
4 mm hollow	0	1.84	1.50	1.64	39.13
Nominal	65	1.36	1.13	1.25	15.91
2 mm hollow	65	1.41	1.12	1.28	19.50
3 mm hollow	65	1.43	1.11	1.36	19.59
4 mm hollow	65	1.62	1.26	1.49	30.80
Nominal	120	1.23	1.07	1.25	8.47
2 mm hollow	120	1.12	1.02	1.18	11.92
3 mm hollow	120	1.09	1.02	1.16	15.81
4 mm hollow	120	1.31	1.10	1.42	26.47
Normalised Limit value		2.08	2.09	2.93	

Table 3: Influence of wheel and rail contact geometry on rail and sleeper stresses and sleeper–ballast contact pressure. The calculated values have been normalised with respect to the corresponding values for nominal sleeper support conditions and wheel–rail contact geometry. Orange text indicates the worst case load scenario proposed for the optimisation of crossing panel design.

presented in Table 4. For Case I, the stress along the most loaded rib and the stress along the sleeper are presented in Figures 5a and 5b, respectively. The stresses are plotted for the longitudinal wheel position where the maximum stress occurs in each simulation. For the sleeper, it is observed that the two models where the crossing rail is modelled either by beam elements or by 3D solid elements lead to very similar results. In this case, it is argued that the difference is mainly attributed to the difference in the model of the rail fastening, see [8]. As expected, for the crossing rail, there is a significant difference between the two models. The more detailed model of the crossing rail leads to significantly higher stresses. The ratio between the calculated maximum stresses is referred to as the notch factor K_t (stress concentration factor) in Table 4.

5 Discussion

By combining the scenarios in Tables 2 and 3, the worst case dynamic load scenarios for each structural requirement is explored together with the corresponding limit value, see Table 4. It is observed that the load limits for sleeper–ballast contact pressure and sleeper bending stress are both violated by at least one of the load scenarios. Differences can be seen between the beam and 3D models developed in [7] and [8], respectively. A lower bending stress in the sleeper is generally noted for the 3D model compared to the beam model. As discussed in Section 4, this discrepancy originates from the difference in the model of the connection between the crossing rail and the
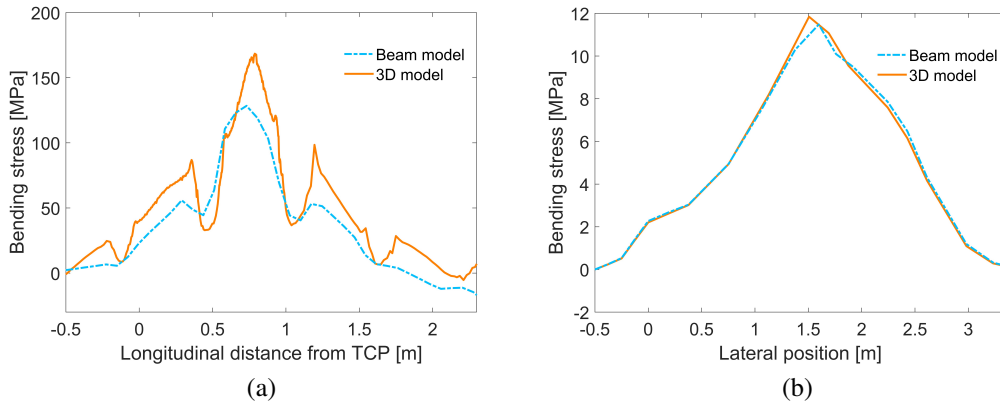
Figure 5: a) Stress along the longitudinal coordinate in the most loaded rib of the crossing rail. The maximum stress in the beam and 3D models is 128 and 168 MPa, respectively, cf. Table 4. b) Stress in the sleeper along the lateral direction. The maximum stress in the beam and 3D models is 12.3 and 11.5 MPa, respectively.

sleeper, which is done with two springs in the 3D model and with one spring in the beam model. The opposite effect can be seen for the crossing rail stress, where the notch factor caused by the varying geometry on the bottom of the crossing rail is neglected in the beam model, leading to lower bending stresses in the beam model than in the 3D model. In addition, this factor may vary depending on the longitudinal position of the wheel transition from wing rail to crossing rail, which varies with different combinations of wheel and rail profiles.

The crossing rail is commonly casted. In the production process, the design of the reinforcements on the bottom of the crossing rail is allowed to vary significantly and is ultimately decided by the individual foundries to facilitate the casting process. This results in slightly varying designs depending on the foundry. It should be noted that the 3D model used in this paper 3D model is based on one of these designs. It is probable that a different design of the crossing rail may affect the notch factor and thus the stress results.

According to Table 4, the sleeper is the component at most risk, while the crossing rail does not exceed the requirement value even with the extreme character of the considered worst case load scenarios. However, the limits are formulated to prevent crack initiation for the sleeper and fatigue failure for the crossing rail, meaning that the two limits are not directly comparable. The character of the structural requirement on the contact stress on the ballast surface is different to the other two in the sense that exceeding the requirement leads to a slow deterioration (differential settlement) of the sleeper support conditions instead of an instantaneous failure. Thus, in a structural optimisation, it would be suitable to also include a penalty function based on the contact stress on the ballast that captures the nonlinear behaviour of settlement.

Worst case	σ_{sleeper} [MPa]	σ_{ballast} [kPa]	σ_{crossing} [MPa]	K_t [-]
Nominal (Beam)	5.08	143	59	
Nominal (3D)	4.60	150	89	1.51
Case I (Beam)	12.32	165	128	
Case I (3D)	11.48	170	168	1.31
Case II (Beam)	10.36	404	109	
Case II (3D)	10.48	416	150	1.38
Case III (Beam)	13.05	231	122	
Case III (3D)	11.76	231	155	1.27
Case IV (Beam)	10.76	166	109	
Case IV (3D)	10.12	167	133	1.23
Limit value	10.56	300	173 (200)	

Table 4: Maximum values evaluated from time histories of calculated sleeper stress, sleeper–ballast contact pressure and crossing rail stress for the different sleeper support cases according to Table 2. Red text indicates violation of the various structural requirements specified in Section 3. Limit value for crossing rail stress is shown for both manganese steel and in parenthesis for UIC 60 rail steel. The notch factor K_t indicates the ratio between crossing rail stresses evaluated with the 3D and beam models.

6 Conclusions

In this paper, structural load limits and four dynamic load case scenarios for railway crossing panel design have been proposed. In addition, it is suggested that the load on the ballast should be limited by a penalty function, giving an incentive to reduce sleeper–ballast contact pressure and settlement. Three of the load scenarios can be considered as extreme cases where violation of the load limits for at least one of the components in the investigated reference crossing panel design can be expected, while the fourth is a more common case where failure is not expected. Several combinations of wheel and rail contact geometries and sleeper support conditions observed in field have been simulated to assess how the resulting dynamic vehicle–track interaction relates to the load limits for each structural components. The established load cases (I – IV in Table 4) were constructed by combining a nominal crossing rail geometry, a hollow worn wheel profile with 4 mm of wear and four different cases of field observed sleeper support conditions. The load limits and the first three load cases can be used in a structural optimisation as constraints and dimensioning load case for each component, respectively.

In parallel, two different models of the crossing panel have been compared. The difference between the models is the modelling of the crossing rail, where one uses beam elements while the other uses 3D solid elements. For the investigated reference crossing panel design, the comparison reveals that all of the proposed load limits are exceeded or nearly exceeded when tested against the constructed field-based dynamic load scenarios. In addition, the comparison highlights the importance of the more

detailed 3D model as the crossing rail stress differs greatly between the models due to the significant notch factor. While there is an imbalance in the requirements in the sense that the sleeper load limit is generally at higher risk to be exceeded than the other requirements, the different limit values are not directly comparable as they limit different types of failure.

Acknowledgements

References

[1] Nicklisch D, Kassa E, Nielsen JCO, et al. Geometry and stiffness optimization for switches and crossings, and simulation of material degradation. Proceedings of the Institution of Mechanical Engineers, Part F: Journal of Rail and Rapid Transit. 2010;224(4):279–292. https://doi.org/10.1243/09544097JRRT348.

[2] Pålsson BA. Optimisation of railway crossing geometry considering a representative set of wheel profiles. Vehicle System Dynamics. 2015;53(2):274–301. https://doi.org/10.1080/00423114.2014.998242.

[3] Grossoni I, Bezin Y, Neves S. Optimisation of support stiffness at railway crossings. Vehicle System Dynamics. 2017; 11;56:1–25. https://doi.org/10.1080/00423114.2017.1404617.

[4] Lau A. Numerical simulation of switch and crossing towards an optimized turnout design, Norwegian University of Science and Technology, Trondheim, Norway, PhD thesis, 2018.

[5] Wan C, Markine V, Shevtsov I. Optimisation of the elastic track properties of turnout crossings. Proceedings of the Institution of Mechanical Engineers, Part F: Journal of Rail and Rapid Transit. 2016;230(2):360–373. https://doi.org/10.1177/0954409714542478.

[6] Jenkins H, Stephenson J, Clayton G, et al. The effect of track and vehicle parameters on wheel/rail vertical dynamic forces. Railway Eng J. 1974; 3(1);2-16.

[7] Pålsson BA, Vilhelmson H, Ossberger U, et al. Dynamic vehicle–track interaction and loading in a railway crossing panel – Calibration of a structural track model to comprehensive field measurements. Vehicle System Dynamics. 2024;1–27. https://doi.org/10.1080/00423114.2024.2305289

[8] Vilhelmson H, Pålsson BA, Nielsen JCO, et al. Dynamic vehicle–track interaction and structural loading in a crossing panel – Calibration and assessment of a model with a 3D representation of the crossing rail. Vehicle System Dynamics. 2024;1–23. https://doi.org/10.1080/00423114.2024.2319275

[9] In2Track. Deliverable 1.1 Enhanced S&C whole system analysis, design and virtual validation (midterm report); 2021.

[10] Craig RR, Bampton MCC. Coupling of substructures for dynamic analyses. AIAA Journal. 1968;6(7):1313–1319. https://doi.org/10.2514/3.4741.

[11] Knothe K, Grassie S. Modelling of railway track and vehicle/track interaction at high frequencies. Vehicle System Dynamics. 1993;22(3-4):209–262. https://doi.org/10.1080/00423119308969027.

[12] Berggren EG, Nissen A, Paulsson BS. Track deflection and stiffness measurements from a track recording car. Proceedings of the Institution of Mechanical Engineers, Part F: Journal of Rail and Rapid Transit. 2014;228(6):570–580. https://doi.org/10.1177/0954409714529267.

[13] Le Pen L, Milne D, Thompson D, et al. Evaluating railway track support stiffness from trackside measurements in the absence of wheel load data. Canadian Geotechnical Journal. 2016;53(7):1156–1166. https://doi.org/10.1139/cgj-2015-0268.

[14] Pålsson BA, Ambur R, Sebès M, et al. A comparison of track model formulations for simulation of dynamic vehicle–track interaction in switches and crossings. Vehicle System Dynamics. 2023;61(3):698–724. https://doi.org/10.1080/00423114.2021.1983183.

[15] Iwnicki S. Manchester benchmarks for rail vehicle simulation. Vehicle System Dynamics. 1998;30(3-4):295–313. https://doi.org/10.1080/00423119808969454.

[16] Meyer J-E, Eriksson C, Holmberg M, UHtsv. Spårväxel – Teknisk specifikation spårväxeltyp 60E, standard rörande trafikverkets spårväxlar (Turnout - Technical specification turnout type 60E, standard regarding turnouts of the Swedish Transport Administration, in Swedish), ctm 199 106. Trafikverket (The Swedish Transport Administration). 2019.

[17] Trvinfra-00007, Ban- och stationsutformning, spårväxelprojektering (Track and station design, turnout planning, in Swedish), version 4.0. Trafikverket (The Swedish Transport Administration). 2022.

[18] Hammar A, UHtsv. Teknisk kravspecifikation, leverans av betongsliprar inklusive slipermatta till spårväxlar 60E (Technical specification, delivery of concrete sleepers including under sleeper pad for turnouts 60E, in Swedish), ctm 196861. Trafikverket (The Swedish Transport Administration). 2018.

[19] European committee for standardization. EN 13230-2:2016, Railway applications – Track – Concrete sleepers and bearers – Part 2: Prestressed monobloc sleepers

[20] Dahlberg, T. Some railroad settlement models- A critical review. Proceedings of the Institution of Mechanical Engineers, Part F: Journal of Rail and Rapid Transit, 2001; Vol. 215, 289-300.

[21] Abadi T, Le Pen L, Zervos A, et al. A review and evaluation of ballast settlement models using results from the Southampton railway testing facility (SRTF). Procedia Engineering. 2016;143,999-1006. https://doi.org/10.1016/j.proeng.2016.06.089.

[22] Sato Y. Optimization of track maintenance work on ballasted track. Proceedings of the World Congress on Railway Research (WCRR '97), 1997;405–411. Florence, Italy.

[23] Esveld C. Modern railway track. MRT-Productions, The Netherlands. 1989.

[24] Lichtberger B, Track Compendium, Eurail press, Germany. 2011,

[25] Larsson A, Johansson RM. Detektorer. Hantering av larm samt åtgärder efter konstaterade skador (Detectors. Handling of alarms and measures following confirmed damage, in Swedish). Trafikverket (The Swedish Transport Administration) 2020.

[26] Kleinert U. DB Oberbauberechnung. Deutsche Bahn. 1992.

[27] Liu X, Markine VL. Train hunting related fast degradation of a railway crossing – condition monitoring and numerical verification. Sensors. 2020;20(8),2278. https://www.mdpi.com/1424-8220/20/8/2278.

[28] Le Pen L, Watson G, Hudson A, et al. Behaviour of under sleeper pads at switches and crossings – Field measurements. Proceedings of the Institution of Mechanical Engineers, Part F: Journal of Rail and Rapid Transit. 2018;232(4):1049–1063. PMID: 30662165; https://doi.org/10.1177/0954409717707400.

[29] Wheeler L, Take W, Hoult N, et al. Use of fiber optic sensing to measure distributed rail strains and determine rail seat forces under a moving train. Canadian Geotechnical Journal. 2019;56(1):1–13. https://doi.org/10.1139/cgj-2017-0163.

[30] Sysyn M, Nabochenko O, Kovalchuk V. Experimental investigation of the dynamic behavior of railway track with sleeper voids. Railway Engineering Science. 2020;28(3):290–304. https://doi.org/10.1007/s40534-020-00217-8.

[31] Milošević MD, Pålsson BA, Nissen A, et al. Condition monitoring of railway crossing geometry via measured and simulated track responses. Sensors. 2022;22(3), 1012. https://www.mdpi.com/1424-8220/22/3/1012.

[32] Zwanenburg WJ. Degradation processes of switches & crossings. IET Conference Proceedings. 2006 January;115–119(4) https://digital-library.theiet.org/content/conferences/10.1049/ic 20060054.